Physics of Phonon-Polaritons in Amorphous Materials

Luigi Casella,[1, a)] Matteo Baggioli,[2, b)] Tatsuya Mori,[3, c)] and Alessio Zaccone[4, 5, 6, d)]
[1)]*Department of Physics "A. Pontremoli", University of Milan, via Celoria 16, 20133 Milan, Italy.*
[2)]*Instituto de Fisica Teorica UAM/CSIC, c/Nicolas Cabrera 13-15, Universidad Autonoma de Madrid, Cantoblanco, 28049 Madrid, Spain.*
[3)]*Division of Materials Science, University of Tsukuba, 1-1-1 Tennodai, Tsukuba, Ibaraki 305-8573, Japan*
[4)]*Department of Physics "A. Pontremoli", University of Milan, via Celoria 16, 20133 Milan, Italy.*
[5)]*Department of Chemical Engineering and Biotechnology, University of Cambridge, Philippa Fawcett Drive, CB30AS Cambridge, U.K.*
[6)]*Cavendish Laboratory, University of Cambridge, JJ Thomson Avenue, CB30HE Cambridge, U.K.*

(Dated: 25 November 2020)

The nature of bosonic excitations in disordered materials has remained elusive due to the difficulties in defining key concepts such as quasi-particles in the presence of disorder. We report on an experimental observation of phonon-polaritons in glasses, including a prominent boson peak (BP), i.e. excess of THz modes over the Debye law. A theoretical framework based on the concept of diffusons is developed to describe the broadening linewidth of the polariton due to disorder-induced scattering. It is shown here for the first time that the BP frequency and the Ioffe-Regel (IR) crossover frequency of the polariton collapse onto the same power-law decay with the diffusivity of the bosonic excitation. This analysis dismisses the hypothesis of the BP being caused by a relic of the van Hove singularity. The presented framework establishes a new methodology to analyze bosonic excitations in amorphous media, well beyond the traditional case of acoustic phonons, and establishes the IR crossover as the fundamental physical mechanism behind the BP.

I. INTRODUCTION

The low-energy vibrational spectra of solids provide direct insights into the complex many-body atomic and molecular dynamics of materials[1]. Understanding the vibrational spectra is crucial for our understanding and technological design of the optical, thermal and mechanical properties of solids. Substantial experimental and theoretical efforts have focused on the case of phonons in amorphous materials, where phonons are well-defined quasiparticles only in the limit of long wavelengths. On shorter length-scales, disorder dominates the vibrational excitations and gives rise to deviations from Debye's quadratic law in the vibrational density of states (VDOS), resulting in the boson peak in the Debye-normalized VDOS, detected originally in Raman scattering spectra[2]. A line of research has traditionally supported the identification of the BP with shifted and smeared van Hove (VH) singularities[3,4]. However, recent studies have pointed out that the boson peak may be largely independent, and in fact even unaffected by the lowered VH singularity. This is indicated by the co-existence of the BP with the lowest (transverse) VH singularity in the spectra of simple models systems[5–7].

Another line of research points at the close link between BP and the Ioffe-Regel (IR) crossover between ballistic phonons and quasi-localized excitations[8–10], as the origin of the BP. Among the theoretical frameworks, the most popular is the heterogeneous elasticity theory of Schirmacher, Ruocco and co-workers[11–13] based on the assumption of spatial correlations in the shear elastic modulus, in agreement with simulations[13]. The original Schirmacher theory, however, is based on the assumption of gaussian fluctuations of the elastic modulus within isotropic elasticity and fails to capture the logarithmically enhanced Rayleigh scattering in the THz regime that is ubiquitously observed in simulations and experiments[14]. A more physical theory based on long-ranged power-law elastic correlations and locally anisotropic elasticity has successfully predicted the logarithmic Rayleigh scattering as observed experimentally[15].

Although growing consensus is emerging about the crucial role of *randomness* in driving the IR crossover from ballistic to quasi-localized excitations leading to a BP, a picture supported by random matrix theory[16–18], the physical origin of the BP remains controversial. This is especially true in light of the recent prediction of the boson peak occurring in perfectly ordered crystals due to a Ioffe-Regel crossover driven by (Akhiezer) anharmonic damping of the phonons[19]. This theoretical prediction has found experimental confirmation in different systems[20–22]. Furthermore, it remains to be established whether the BP is a distinctive feature of the *acoustic* phonon spectra only, or if it is a more general phenomenon common to all bosonic-like excitations in amorphous solids (e.g. excitons, plasmons, polaritons).

Here we provide an answer to these fundamental questions by reporting on the experimental observation and analysis of the BP in infrared absorption spectra of phonon-polaritons in a model glass, i.e. soda-lime silicate.

We support the analysis with a theory of phonon-polaritons

[a)]Electronic mail: luigi.casella@studenti.unimi.it
[b)]Electronic mail: matteo.baggioli@uam.es
[c)]Electronic mail: mori@ims.tsukuba.ac.jp
[d)]Electronic mail: alessio.zaccone@unimi.it

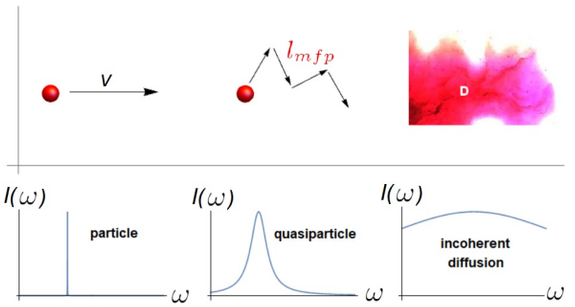

FIG. 1. Visual representation of the destruction of the quasiparticles coherence induced by disorder-induced scattering events. In the top panel, the salient dynamics of the excitations, and in the bottom panel the corresponding pattern observed in the scattering intensity $I(\omega)$ of the excitation, are schematically depicted. For growing disorder in the sample, upon going from left to right, the dynamics of the system becomes incoherent. The mean free path (ℓ) of the quasiparticles becomes eventually shorter than the wavelength resulting in a diffusive-like propagation, with diffusion constant D, through the sample. In this regime, the low frequency dynamics is well described by hydrodynamics.

in amorphous materials. This theoretical framework clarifies the origin of the BP from the IR crossover between the ballistic quasi-particle (coherent) propagation to a quasi-localized regime dominated by disorder-induced scattering. In this regime, the quasiparticle loses its coherence and undergoes diffusive-like dynamics (*diffusons*)[7,10,23] (see Fig.1). This claim is supported by showing that the IR frequency and the BP frequency of the polariton collapse onto the same power-law as a function of the phonon (Akhiezer) diffusivity parameter, in excellent agreement with the theoretical prediction.

These results show the that the BP is a truly universal feature for all bosonic excitations in amorphous materials, not just acoustic phonons. Also, the theoretical analysis shows that the BP does not originate from the flattening of the polariton dispersion relations, thus ruling out the lowered VH singularity as a possible origin of the BP.

II. THEORETICAL MODEL

We start by modelling the coupled dynamics of the optical phonon modes and the EM field. Following the seminal work of Born and Huang[1,24,25], the first step is to define the relative displacement field $\vec{u} = \vec{u}_+ - \vec{u}_-$, that accounts for the relative displacement of the positive and negative partial charges in the solid. With this definition we can study the dynamical equation for this field,

$$\ddot{\vec{u}} = -\omega_0^2 \vec{u} + f(\dot{\vec{u}}) + b_{12}\vec{E}. \tag{1}$$

where b_{12} is a parameter describing the effective coupling between the atomic displacement field and the EM field[1].

The relative displacement field characterizes the relative motion of the partially-charged particles and applies to optical (and not acoustic) vibrational modes. The first term in the r.h.s. of Eq.(1) defines the characteristic frequency of the harmonic oscillator, which originates from the linear restoring force acting on the atoms. The second term is the damping contribution, where f is some function. The last term is a direct dipole coupling to the external electric field $\vec{E}$ due to the partial charge carried by the atoms.
In the absence of damping, $f(\dot{\vec{u}}) = 0$, this problem was considered in Refs.[1,25] where Eq.(1) was solved together with an equation for the polarization that contains the effects of the relative displacement of the atoms, and with the Maxwell equations for the EM field. Notice that damping is introduced in Eq.(1) only in the mechanical part of the equations but not in the EM sector. Assuming a (Langevin-type) damping force linear in the velocity of the displacement field, as is customary for dissipative dynamics in condensed matter[26], and with a coefficient dependent on the wavelength of the oscillation ($f(\dot{\vec{u}}) = \Gamma(k)\,\dot{\vec{u}}$), we solve the dynamical problem with damping Eq.(1) and obtained a quartic equation for the transverse optical (TO) modes $\omega_{TO}(k)$, which reads:

$$\begin{aligned}&\omega_{TO}^4\,\varepsilon_\infty + i\,\omega_{TO}^3\,\Gamma(k)\,\varepsilon_\infty - \omega_{TO}^2\left(\omega_0^2\,\varepsilon_0 + k^2c^2\right)\\&- i\Gamma(k)\,k^2c^2\omega_{TO} + \omega_0^2\,k^2\,c^2 = 0.\end{aligned} \tag{2}$$

The label TO, to simplify the notation, will be dropped in the rest of this manuscript.
In the above Eq.(2), c is the speed of light, ω_0 the characteristic frequency (the energy gap of the optical mechanical mode), and $\varepsilon_0, \varepsilon_\infty$ are the dielectric constants at zero and infinite frequency, respectively. Finally, $\Gamma(k)$ accounts for all the damping effects on the oscillations. The details of the derivation of Eq.(2) can be found in the Appendix B.

Equation (2) can be viewed in two different ways. First, one can assume the momentum k to be real, and the frequency to be complex. In this framework, the modes $\omega(k) = \mathrm{Re}\,\omega(k) + \mathrm{i}\,\mathrm{Im}\,\omega(k)$ are usually referred to as *quasi-normal modes* and the imaginary part of the frequency determines their exponential decay in time $\sim e^{-\mathrm{Im}\omega(k)t}$. Alternatively, one could take the frequency as real and the momentum to be complex. In this case Eq.(2) can be solved for $k(\omega)$ and the imaginary part of the momentum determines the exponential decay in space $\sim e^{-\mathrm{Im}k(\omega)x}$, i.e. the penetration length. The two scenarios are interchangeable. In the rest of the manuscript we will use the abbreviations $\mathrm{Re}\,k \equiv k'$ and $\mathrm{Im}\,k \equiv k''$.

Let us notice that our formalism is an effective field description, which is agnostic about the microscopic physics and it is valid only on length scales larger than that. The damping parameter $\Gamma(k)$ is a phenomenological coefficient whose fundamental origin is not (and cannot be) discussed without resorting to complicated many-body treatments or heavy numerics. In this sense, it includes all the possible effects related to incoherence, scattering processes and attenuation mechanisms making our description very general.

By using the standard linear relation between $\vec{P}$ and $\vec{E}$, coupled with Eq.(1), we can derive the *dielectric function* (see Appendix B for details),

$$\varepsilon(\omega,k) = \varepsilon_\infty - \frac{\omega_0^2\,(\varepsilon_0-\varepsilon_\infty)}{\omega^2-\omega_0^2+i\,\omega\,\Gamma(k)}. \tag{3}$$

Furthermore, by studying the spatial exponential attenuation (Lambert-Beer) of the wave intensity I,

$$I/I_0 = e^{-\alpha(\omega)x} = e^{-2k''(\omega)x} \tag{4}$$

we can define the *absorption coefficient* $\alpha(\omega)$, which is the inverse of the *penetration length*[27]. Given a collection of scattering centers, the mean free path is given by $\ell = (\sigma n)^{-1}$, where σ is the scattering cross-section and n the number density of scatterers. It can be shown[27] that $dI/dx = -In\sigma = -I/\ell$, leading to exponential attenuation $I \sim \exp(-x/\ell)$. Upon comparing this with the above equation, we thus obtain

$$\ell^{-1} = 2k''(\omega) \tag{5}$$

a relation that will be useful also later on.

An expression for the absorption coefficient can be derived using the complex dielectric function for EM radiation in continuous media[28], $\varepsilon_{EM}(\omega) = c^2k^2/\omega^2$. Solving this expression for k, and taking the imaginary part (see Eq. (4)), we find:

$$\alpha(\omega) = \frac{\omega}{c}\sqrt{2\,(|\varepsilon(\omega)| - \mathrm{Re}\,\varepsilon(\omega))}. \tag{6}$$

At this point, it is crucial to specify the nature of the linewidth $\Gamma(k)$, which is neglected in standard treatments[24,25]. The linewidth encodes the effects of the disorder on the propagation of the polariton. The basic idea is that disorder can be represented as a large number of "defects", each acting on the polariton quasiparticle as a scattering center. On length-scales larger than the defects average separation, the result of a large number of scattering events is the diffusion of momentum through the system. This effective description is based on the idea of *diffusons*[23,29], a concept which proved useful in explaining the anomalies in thermal transport observed experimentally in glasses[30]. A diffusive linewidth for phonons can indeed explain the ubiquitous appearance of a boson peak in the vibrational density of states (VDOS) of glasses[7,31] and even the presence of a linear in T term in the specific heat at low T, as shown in Ref.[32]. Moreover, the diffusive nature of the linewidth is supported by Random Matrix Theory[18,33].

Following Refs.[7,9,33], we take the linewidth to be of diffusive form

$$\Gamma(k) = Dk^2 \tag{7}$$

which follows from an effective hydrodynamic treatment[34] for quasiparticle excitations or simply from diffusion of momentum in the governing dynamic equation for the displacement field[7]. This expression is supported by experiments and simulations[9,10,35–37] and is valid only at relatively low k, while it is expected to break down at larger momenta where hydrodynamics is no longer a good approximation[38].

In Fig.10 of the Appendix B, we show the Debye-normalized absorption coefficient obtained from this model for a wide range of values of the diffusion coefficient D. The absorption coefficient is directly proportional, up to a linear growing function of the frequency denoted as[39–41] $C(\omega)$, to the VDOS. As a consequence, an excess in $\alpha(\omega)/\omega^2$ corresponds to a boson peak in the normalized VDOS, $g(\omega)/\omega^2$. We observe that the BP moves to lower energies by increasing the diffusion constant D and it becomes sharper. In the inset, we show the dispersion relation of the corresponding phonon-polariton modes obtained from Eq.(2) and we compare it with the BP frequency ω_{BP}. This dynamics and the underlying physics mechanism will be discussed in detail later.

III. COMPARISON WITH EXPERIMENTAL DATA

The linewidth ceases to display a hydrodynamic diffusive behaviour as in Eq.(7) at large momenta approaching the molecular size. We observe (see Fig. 6 in the Appendix B) that the high-frequency part of the experimental spectra is well-fitted by a constant damping coefficient: $\Gamma(k) = \gamma = const$, which corresponds to a microscopic Langevin friction term in Eq.(2), as expected in local molecular-level dynamics in glassy environment. Indeed, on small length-scales, we cannot coarse-grain the effects of disorder into a hydrodynamic description but we have to consider the high-frequency microscopic dynamics[16] producing a k-independent relaxation time $\tau^{-1} \sim \gamma$.

In order to have a good description of the experimental data across the entire range of momenta, we will consider a linewidth which interpolates from the diffusive form (7) at low k to the Langevin-like constant damping γ at large k. More specifically, we use an interpolating model of the form:

$$\Gamma(k) = \frac{\gamma D k^2}{\gamma + Dk^2} \tag{8}$$

which retrieves the two limits. We test our theoretical model using experimental measures of the infrared absorption spectra on a soda-lime glass sample using two different THz time-domain spectrometers that can cover a wide frequency range 0.3 – 5 THz (see Appendix A for details).
By implementing Eq.(2) and Eq.(8) into Eq.(3), and the latter into Eq.(6), we obtain the theoretical predictions shown in comparison with experimental data in Fig.2. The *diffusons* behaviour at low k is crucial to obtain a good agreement at low frequencies and we checked that it cannot be described with a simple damped harmonic oscillator (DHO) model as shown in Fig. 6 in the Appendix B. It is also to be noted that the decay at large ω is dominated by the constant damping γ.

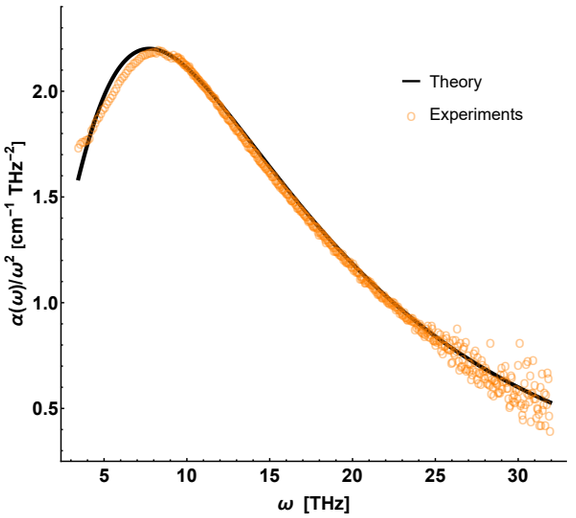

FIG. 2. The comparison between the theoretical model based on the diffusive linewidth function Eq.(8) (black line) and the experimental data for a soda lime glass (orange circles). The fit gives: $D = 13.99$ THz$^{-1}/c^2$, $\gamma = 69.67$ THz^{-1}, $\varepsilon_0 = 70.99$, $\varepsilon_\infty = 61.11$, $\omega_0 = 29.80$ THz.

IV. THE ORIGIN OF THE BOSON PEAK

Our effective theoretical model gives an accurate qualitative description of the experimental data and it is able to reproduce the boson peak. We should now address the question of the fundamental physical origin of the BP in the polariton spectra. Let us recall that the BP frequency is defined as

$$\omega_{BP}: \qquad \frac{d}{d\omega}\frac{\alpha(\omega)}{\omega^2}\Big|_{\omega_{BP}} = 0 \tag{9}$$

and it corresponds to the maximum in the Debye-normalized absorption spectra.

A possible explanation for the BP could come from the flattening of the phonon-polariton band:

$$\omega_{flat}: \qquad \frac{d\omega}{dk}\Big|_{\omega_{flat}} = 0 \tag{10}$$

which, similarly to the van Hove singularities in ordered crystals, would produce a peak in the VDOS since $g(\omega) \sim (d\omega/dk)^{-1}$, see Ref.[42]. As one can readily verify in Fig.6 of Appendix B, the position of the BP does not correspond to the flattening of the lowest branch. Hence, the flattening of the polaritonic dispersion relations cannot satisfactorily explain the occurrence of the BP.

From a different perspective, it is well-known that waves in amorphous and disordered systems stop to propagate ballistically at a certain frequency known as the Ioffe-Regel frequency[43], ω_{IR}. Moreover, the correlation between the Ioffe-Regel frequency and the BP frequency has been observed and discussed in recent works[8–10].

The Ioffe-Regel frequency[43] is defined as the energy at which the mean free path of the wave ℓ becomes comparable to its wavelength λ,

$$\ell(\omega_{IR}) = \lambda(\omega_{IR}) \tag{11}$$

and its quasiparticle nature is lost. Upon combining Eq. (11) with Eq. (5) and $k' = 2\pi/\lambda$, we obtain

$$\omega_{IR}: \qquad k'(\omega_{IR}) = 4\pi k''(\omega_{IR}) \tag{12}$$

which provides a new operational quantitative definition of the Ioffe-Regel frequency for a generic collective excitation.

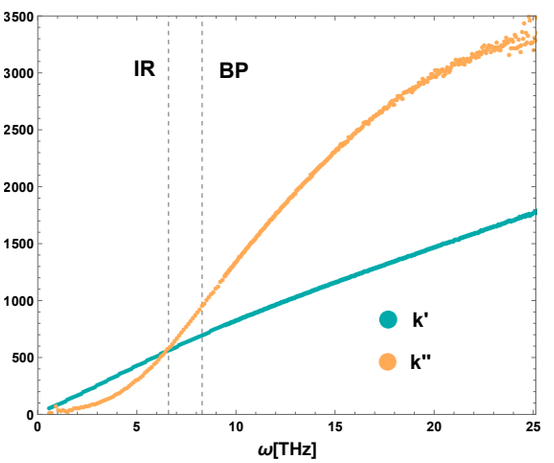

FIG. 3. The experimental data for $k(\omega)$ in the soda lime glass (see Fig.5 in the Appendix A). The units are cm^{-1} for the momentum k and THz for the frequency ω. The first dashed line indicates the location of the IR frequency defined from Eq. (12); the second dashed line indicates the BP position which can be found from the absorption data in Fig.2. We find that $\omega_{BP}/\omega_{IR} \approx 1.25$, confirming the results of Eq.(13).

In Fig.3, we show the experimental data of $k(\omega)$ for the soda lime glass (see more details in the Appendix A). From there it is evident that the Ioffe-Regel crossover, defined using Eq.(12), is extremely close to the BP frequency observed in the absorption (Fig.2), $\omega_{BP}/\omega_{IR} \sim 1.25$. This represents a strong experimental confirmation of the intimate correlation between the BP and the IR frequencies in the phonon-polariton spectrum of glasses.

In order to emphasize this point, we compare the BP frequency ω_{BP} and the Ioffe-Regel frequency ω_{IR} for the theoretical model in Fig.4. This procedure was carried out numerically. Nevertheless, given a (reasonably simple) linewidth function $\Gamma(k)$, the correlation can be derived analytically since it depends solely on the function $k(\omega)$, from inversion of Eq.(2).

We again observe that the two values strongly correlate:

$$\omega_{BP} = \mathscr{C}\,\omega_{IR} \tag{13}$$

where $\mathscr{C}$ is an $\mathscr{O}(1)$ constant prefactor. From the soda lime glass experimental data we consistently find $\mathscr{C} \approx 1.25$ (see

Fig.3).

Importantly, we also find that both frequencies collapse onto the same power law scaling $\omega \sim D^{-n}$ with $n \approx 0.32$, which is a new physical scaling never shown before. More broadly, we expect Eq.(13) to hold in general, up to a non-universal $\mathscr{O}(1)$ prefactor $\mathscr{C}$, that is different for different materials.

This analysis brings a new point in the discussion about the origin of the BP. As we have mentioned in this section above, the BP is present even with strong phonon-diffusion processes. Here stands the major point in dismissing the van Hove singularity hypothesis, i.e. the presence of the peak in a regime for which the dispersion relations do not display any flattening. What our theoretical analysis shows, is that the BP is not only present in any phonon diffusion regime, but also its dynamics through the regimes follows closely a power law in the diffusion parameter D, thus revealing a connection between the microscopic phonon diffusion processes (read: long range disorder) and the BP. This connection is than found in the dynamics of the IR crossover, a quantity intrinsically connected to phonon diffusion processes and their interplay with ballistic phonon propagation.

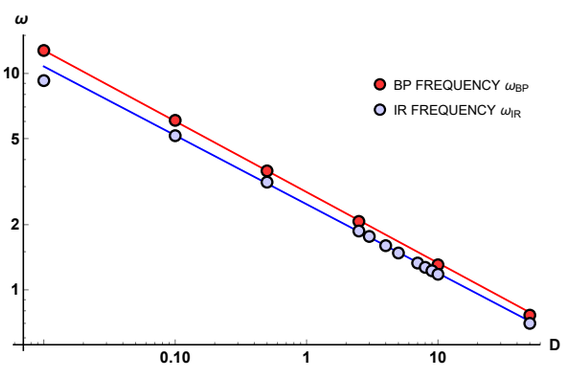

FIG. 4. The BP frequency ω_{BP} and the IR frequency ω_{IR} as a function of the diffusion constant D. The red and blue lines show the fit which at large D is consistent with a scaling $\omega \sim D^{-n}$ with $n \approx 0.32$.

V. CONCLUSIONS

In summary, we reported on the experimental observation and theoretical analysis of phonon-polaritons in a model amorphous material. The polaritonic nature of the excitation cannot be reproduced by standard DHO fitting, but only using a diffusive $\sim k^2$ linewidth. We can confidently claim that the boson peak observed experimentally in the phonon-polariton absorption spectrum is controlled by the Ioffe-Regel crossover from ballistic quasi-particle propagation to incoherent diffusive-like excitations (*diffusons*[23]). This identification, which is valid with high precision, suggests that the physical mechanism underlying the BP in the phonon-polariton spectra of glasses is due to the quasi-localization of the excitations and to the propagating-to-diffusive crossover á la Ioffe-Regel. Working with polaritons has the advantage that we could clearly rule out the influence of dispersion relation band flattening on the peak, away from the influence of pseudo-van Hove singularities, and hence this analysis provides the first unambiguous demonstration that boson peak and Ioffe-Regel crossover frequencies coincide and collapse onto a new power-law scaling with the excitation diffusivity D, discovered here for the first time. Crucially, our results suggest that this mechanism for the BP may apply to *any* bosonic excitations in amorphous materials (such as excitons, magnons, plasmons)[44], which opens up new opportunities for technological design and control of optical, electrical and thermal properties of materials by tailoring the disorder-induced effects.

ACKNOWLEDGMENTS

M.B. acknowledges the support of the Spanish MINECO's "Centro de Excelencia Severo Ochoa" Programme under grant SEV-2012-0249. A.Z. acknowledges financial support from US Army Research Laboratory and US Army Research Office through contract nr. W911NF-19-2-0055. T.M. is grateful to Y. Matsuda for providing the glass sample and acknowledges JSPS KAKENHI Grant Nos. JP17K14318 and JP18H04476, and the Asahi Glass Foundation.

Appendix A: Experimental methods

As a standard glass system exhibiting the BP in the infrared spectrum, we selected a soda-lime glass which is a typical network glass former. The sample is purchased from Central Glass Co., Ltd. We utilized two different commercial THz time-domain spectrometers to cover a wide frequency range between 0.3 – 5 THz (0.3 - 1.2 THz: RT-10000, Tochigi Nikon Co.; 1.2 – 5 THz: TAS7500SU, Advantest Corp.)[41,45–50]. The measured THz waveforms including multiple reflections in the sample surfaces were converted to the frequency domain, and the obtained complex transmission coefficient t was analyzed using the following equation:

$$t(\omega) = t_{vs}\, t_{sv}\, \frac{e^{i(n_s-1)\,d\,\omega/c}}{1 - r_{sv}^2(\omega)\, e^{i2n_s\,d\,\omega/c}}, \qquad \text{(A1)}$$

where:

$$t_{ij} = \frac{2n_i}{n_i + n_j}, \quad r_{ij} = \frac{n_i - n_j}{n_i + n_j} \qquad \text{(A2)}$$

are the complex Fresnel's transmission and reflection coefficients, respectively, at the interface between regions i and j. The subscripts i and j stand for v and s in equation (A1), representing the vacuum and sample, respectively. n_i is the complex refractive index of region i, d is the thickness of sample, and c is the speed of light. The data of n_s were combined with the low-frequency data measured using RT-10000

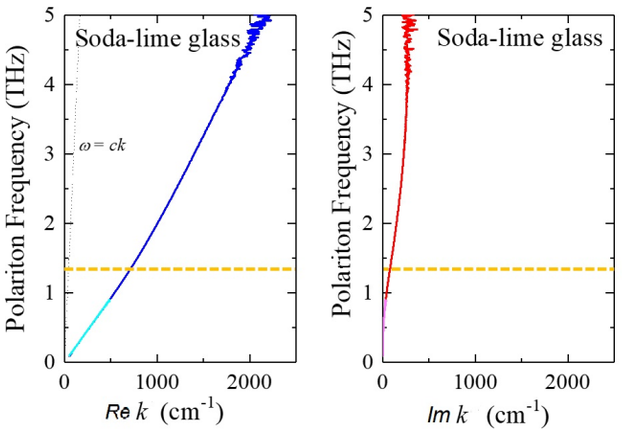

FIG. 5. The dispersion relation of the polariton in the soda-lime glass extracted from the experimental data used in this work. The yellow dashed line indicates the BP frequency $\omega_{BP} \approx 1.32$ THz.

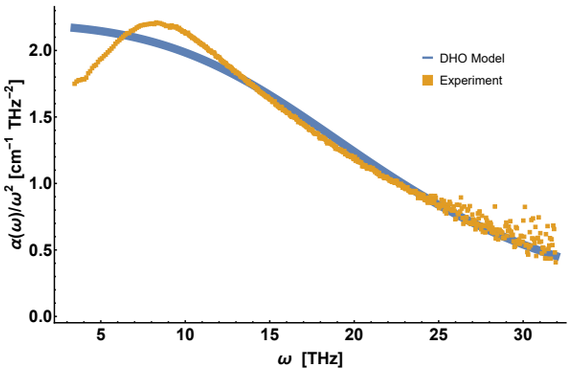

FIG. 6. Absorption (normalized by Debye law) in the THz range. The yellow markers are the experimental data and the blue line is the fit with the constant damping model.

(Tochigi Nikon Co.) and the high-frequency data measured using TAS7500SU (Advantest Corp.) at 1.5 THz[50]. The absolute values of the n_s were obtained based on those observed for the low-frequency side. The square of n_s is the complex permittivity, and the real and imaginary parts of the permittivity are shown in Fig.7.

Then, the infrared absorption coefficient $\alpha(\omega)$ is obtained from the relation:

$$\alpha(\omega) = \frac{2\,\omega\,\kappa(\omega)}{c}, \tag{A3}$$

where $\kappa(\omega)$ is the imaginary part of n_s, i.e. the extinction coefficient. From the linear response theory for disordered systems[39], $\alpha(\omega)$ and the vibrational density of states $g(\omega)$ are related through the infrared photon-phonon coupling coefficient $C_{IR}(\omega)$ as following:

$$\alpha(\omega) = C_{IR}(\omega)\, g(\omega) \tag{A4}$$

The BP appears in the spectrum of $g(\omega)/\omega^2$, therefore the BP in the infrared spectrum appears in the plot of $\alpha(\omega)/\omega^2$. Some experimental data for the dielectric constant are shown in Fig.6 together with the fits from the DHO theoretical model, which shows the latter's deficiencies. Moreover, in Fig.5 we show the dispersion relation of the polariton as extracted from the experimental data.

Appendix B: Theoretical model calibration on experimental data

As discussed in the main text, the damping mechanism is different depending on the frequency range we are looking at. At high energy (frequency/momentum), the microscopic details of the disorder are relevant, and the disorder-induced scattering is well approximated by a constant damping term $\Gamma(k) = \gamma$ as in the Drude model for electron conduction or in the Langevin equation for molecular motion in dense environment. In this regime, the damping is basically provided by the microscopic collisions in the localized motion of atoms. In Fig.6 we show that this damping provides indeed a good approximation for the experimental data but only at large frequencies, much above the boson peak frequency ω_{BP}. At low frequency, the experimental normalized absorption turns down, while the DHO model with a constant damping cannot reproduce such trend.

As explained in the main text, at low frequencies the nature of the linewidth can be well approximated by the hydrodynamic expressions for *diffusons*:

$$\Gamma(k) = Dk^2. \tag{B1}$$

This mechanism comes from a coarse-grained description for which, on sufficiently large length scales, the effects of the microscopic scattering events are encoded in an effective "diffusion" dynamics of the excitations. In order to have control over the full range of frequency, we build an interpolating model:

$$\Gamma(k) = \frac{\gamma D k^2}{\gamma + Dk^2} \tag{B2}$$

which smoothly crosses over between the two, low-k and high-k, regimes. Using this model, we are able to accurately fit the experimental data across the whole range of frequencies. This is emphasized in Fig.7 where the full set of experimental data is shown and compared to our theory.

1. Derivation of the phonon-polariton dispersion relations

In order to derive our main relation Eq.(2), we start by writing down the system of coupled dynamical equations for the relative (partially-)charged-particle displacement field $\vec{u}$, the

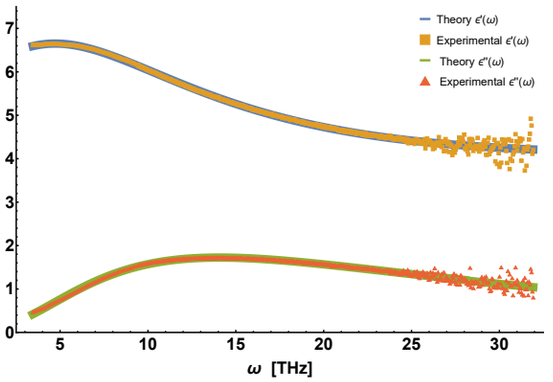

FIG. 7. Dielectric function (real and imaginary part) of the soda lime glass in the THz range. The theoretical model uses the diffusive linewidth model, Eq.(8) in the main text. The plotted values of ε' and ε'' are in arbitrary units.

polarization vector $\vec{P}$ and the EM fields $\vec{E},\vec{H}$.

$$\begin{cases} \ddot{\vec{u}} = b_{11}\vec{u} - \Gamma(k)\dot{\vec{u}} + b_{12}\vec{E} \\ \vec{P} = b_{21}\vec{u} + b_{22}\vec{E} \\ \nabla\cdot(\vec{E}+4\pi\vec{P}) = 0 \\ \nabla\cdot\vec{H} = 0 \\ \nabla\times\vec{E} = -\frac{1}{c}\dot{\vec{H}} \\ \nabla\times\vec{H} = \frac{1}{c}(\dot{\vec{E}}+4\pi\dot{\vec{P}}) \end{cases} \tag{B3}$$

in which we importantly add an effective damping term $\Gamma(k)$ which encodes the effects of disorder and dissipation on the atomic motion. Going to Fourier space and identifying the coefficient b_{11} with the characteristic mechanical oscillation frequency ω_0 as in Ref.[1], the equations can be written as

$$\begin{cases} \vec{u} = -\dfrac{b_{12}}{\omega^2-\omega_0^2+i\omega\Gamma(k)}\vec{E} \\ \vec{P} = \left(b_{22} - \dfrac{b_{12}b_{21}}{\omega^2-\omega_0^2+i\,\omega\Gamma(k)}\right)\vec{E} \\ \vec{k}\cdot\vec{E}\left(1+4\pi b_{22} - \dfrac{4\pi b_{12}b_{21}}{\omega^2-\omega_0^2+i\,\omega\Gamma(k)}\right) = 0 \\ \vec{k}\cdot\vec{H} = 0 \\ \vec{k}\times\vec{E} = \frac{\omega}{c}\vec{H} \\ \vec{k}\times\vec{H} = -\frac{\omega}{c}(\vec{E}+4\pi\vec{P}). \end{cases} \tag{B4}$$

Using the known relation $\vec{D} = \vec{E}+4\pi\vec{P} = \varepsilon(\omega)\vec{E}$, we can substitute the unknown parameters b_{12}, b_{21}, b_{22} in terms of the dielectric constant. We denote:

$$\varepsilon(\omega=0) \equiv \varepsilon_0\,, \qquad \varepsilon(\omega\to\infty) \equiv \varepsilon_\infty \tag{B5}$$

and using these definitions, the third equation in Eq.(B4) can be re-written as:

$$\vec{k}\cdot\vec{E}\left(\varepsilon_\infty - \frac{\omega_0^2(\varepsilon_0-\varepsilon_\infty)}{\omega^2-\omega_0^2+i\,\omega\Gamma(k)}\right) = 0. \tag{B6}$$

At this point, a comment is in order. The scalar product $\vec{k}\cdot\vec{E}$ distinguishes between two different types of modes:

$$\vec{k}\cdot\vec{E} \neq 0 \qquad \to \text{LO modes}\,, \tag{B7}$$
$$\vec{k}\cdot\vec{E} = 0 \qquad \to \text{TO modes}\,. \tag{B8}$$

Starting from the LO modes and assuming $\vec{k}\cdot\vec{E}\neq 0$, the Eq.(B6) implies

$$\begin{aligned} &\varepsilon_\infty = \frac{\omega_0^2(\varepsilon_0-\varepsilon_\infty)}{\omega^2-\omega_0^2+i\,\omega\Gamma(k)} \\ &\omega_{LO}^2 + i\,\omega_{LO}\Gamma(k) - \omega_0^2\frac{\varepsilon_0}{\varepsilon_\infty} = 0 \end{aligned} \tag{B9}$$

where we have indicated the frequency of the mode $\omega=\omega_{LO}$.

Moving on to the TO modes and taking $\vec{k}$ and $\vec{E}$ orthogonal, we can observe from Eq.(B4) that the magnetic field $\vec{H}$ is orthogonal to both the vectors $\vec{k}$ and $\vec{E}$. As a consequence, the fifth and sixth equations in Eq.(B4) become a coupled relation between the amplitudes:

$$\begin{cases} kE = \dfrac{\omega_{TO}}{c}H \\ kH = \dfrac{\omega_{TO}}{c}E\left(\varepsilon_\infty - \dfrac{\omega_0^2(\varepsilon_0-\varepsilon_\infty)}{\omega_{TO}^2-\omega_0^2+i\,\omega\Gamma(k)}\right) \end{cases}$$

$$\Rightarrow \quad k^2c^2 = \omega_{TO}^2\left(\varepsilon_\infty - \frac{\omega_0^2(\varepsilon_0-\varepsilon_\infty)}{\omega_{TO}^2-\omega_0^2+i\,\omega\Gamma(k)}\right). \tag{B10}$$

After simple algebraic manipulations, we finally obtain the quartic equation Eq.(2) presented in the main text:

$$\begin{aligned} &\omega^4\varepsilon_\infty + i\omega^3\Gamma(k)\,\varepsilon_\infty - \omega^2\left(\omega_0^2\varepsilon_0 + k^2c^2\right) \\ &- i\Gamma(k)\,k^2c^2\omega + \omega_0^2k^2c^2 = 0 \end{aligned} \tag{B11}$$

where for simplicity we have omitted the label TO, which stands for transverse optical.

Appendix C: Effects of disorder and damping on the phonon-polariton dispersion relation

We start with the quartic equation which we derived in the previous section

$$\begin{aligned} &\omega^4\varepsilon_\infty + i\omega^3\Gamma(k)\,\varepsilon_\infty - \omega^2\left(\omega_0^2\varepsilon_0 + k^2c^2\right) \\ &- i\Gamma(k)\,k^2c^2\omega + \omega_0^2k^2c^2 = 0 \end{aligned} \tag{C1}$$

where the disorder and damping effects are effectively encoded in the momentum dependent parameter $\Gamma(k)$. Let us start by reminding the reader about the known results in absence of any damping mechanism, $\Gamma(k)=0$, which was derived in Refs.[24,25]. In this simple case, the solution can be written concisely as:

$$\omega = \sqrt{\frac{c^2k^2 \pm \sqrt{c^4k^4 + 2c^2k^2\omega_0^2(\varepsilon_0-2\varepsilon_\infty) + \varepsilon_0^2\omega_0^4} + \varepsilon_0\omega_0^2}{2\,\varepsilon_\infty}} \tag{C2}$$

The two modes display the repulsion phenomenon which is typical of the polariton dynamics and is due to the electromagnetic interactions encoded in the non-trivial dieletric constant ($\varepsilon_\infty \neq \varepsilon_0$). This behaviour is very similar to the one is displayed in panel a) of Figure 8 for a concrete choice of parameters with small damping. Obviously, this is an idealized situation in which all the effects which originate from internal scattering events are neglected.

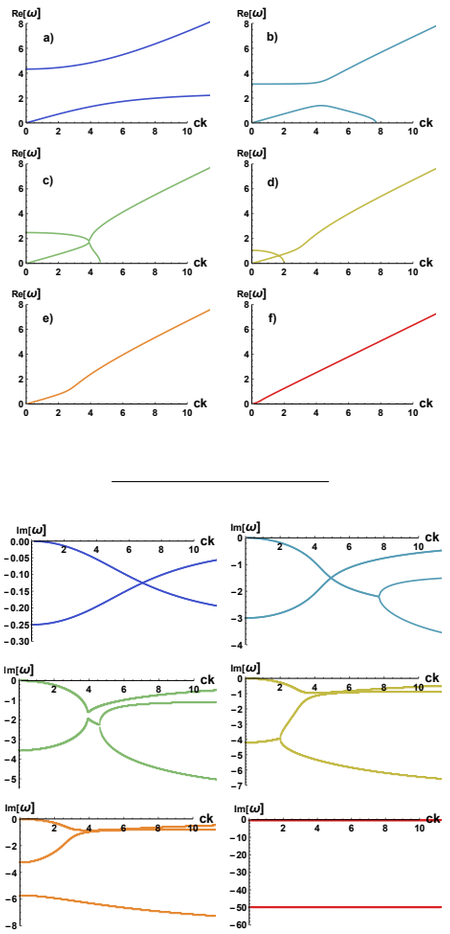

FIG. 8. The dispersion relation of the excitations in the damped model upon changing the damping parameter $\gamma = 0.5, 2.5, 6, 7.1, 8.4, 9, 50$ from panel a) to panel f). **Top:** The real part $\mathrm{Re}(\omega)$ in function of the momentum k. **Bottom:** The imaginary part $\mathrm{Im}(\omega)$ as a function of the momentum k for the same conditions.

As a step forward, let us consider the situation in which the optical phonons have a finite and momentum independent relaxation time:

$$\tau^{-1} = \Gamma(k=0) = \gamma \tag{C3}$$

which determines their lifetime and mean free path. Here, we take an effective field theory perspective and we do not discuss the microscopic origin of this relaxation time. Several are the physical mechanisms that can contribute to this

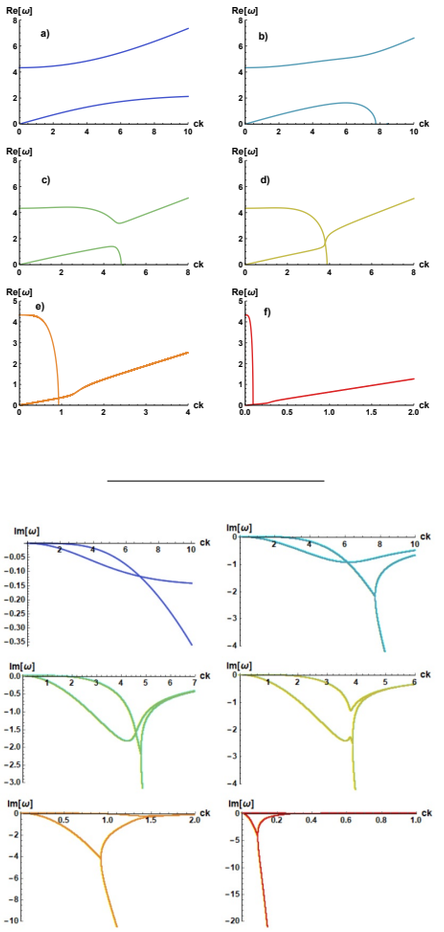

FIG. 9. The dispersion relation of the excitations in the diffusive model upon changing the diffusion constant $D = 0.01, 0.1, 0.3, 0.5, 10, 10^3$ from panel a) to panel f). **Top:** The real part $\mathrm{Re}(\omega)$ as a function of the momentum k. **Bottom:** The imaginary part $\mathrm{Im}(\omega)$ as a function of the momentum k for the same conditions.

effect. Theoretically, this relaxation time implies the non-conservation of momentum, which now dissipates at a rate γ, exactly as in the simple Drude model for electric conduction[42] or in the Langevin equation for Brownian motion in liquids. This relaxation time approximation can be formally derived using Boltzmann equation and kinetic theory[51] and it is valid only in the regime when τ is large enough. The dynamics of the low energy modes is displayed in Fig. 8 upon increasing the relaxation rate $\gamma \in [0, 50]$ from panel a) to panel f). For small $\gamma \ll \omega_0$, the gapless mode acquires a small damping $\mathrm{Im}(\omega)(k=0) \neq 0$ which grows with γ. This mode is not anymore a hydrodynamic mode. The other gapped mode does not acquire a finite damping and remains diffusive at low momentum. When the damping parameter becomes comparable with the characteristic frequency of the gapped mode $\gamma \sim \omega_0$, the two modes attract each other and they move closer as shown in panel b) of Fig.8. When $\gamma \geq 2\omega_0$, the dynamics is not anymore *underdamped* and the modes merge producing a complicated

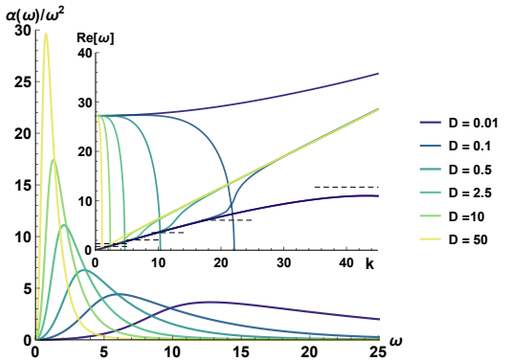

FIG. 10. The Debye normalized absorption coefficient as a function of the frequency ω assuming a diffusive damping $\Gamma(k) = Dk^2$. We vary the diffusion constant D as indicated in the legend. We fix $\varepsilon_\infty = 2.5$, $\varepsilon_0 = 7.5$, $\Omega = 5\pi$. The inset shows the corresponding dispersion relation of the phonon-polariton modes where the dashed horizontal lines indicate the position of the maxima in the absorption – the BP frequency ω_{BP}.

pattern shown in the panels c) and d) of Fig.8. Finally, in the limit $\gamma \gg \omega_0$ (*overdamped* regime), the sound mode gets completely destroyed and it acquires a very large damping. Its lifetime becomes very short and it completely disappears from the dynamics (see panel e) in Fig.8). As a consequence, the "photon component" does not feel anymore the presence of the phonon, and the dispersion relation of the left mode goes back to the free photon case, $\omega = \pm ck$, in which interactions are absent. This last step is shown in panel f) of Fig.8.

Let us consider now a second and different case which will be more relevant for our discussion. More precisely, let us assume that the imaginary part of the vibrational mode is purely diffusive:

$$\Gamma(k) = Dk^2 \tag{C4}$$

The parameter D is the diffusion constant of the diffusons and is determined by elastic scattering events due to the disorder. Importantly, this choice is different with respect to the previous one in several aspects. The presence of diffusion does not imply the non-conservation of momentum[11], nor the explicit breaking of any symmetry. The quasiparticle nature of the optical phonons gets lost across a ballistic to diffusive crossover (Ioffe-Regel crossover)[43]. The phenomenon is shown in Fig.1 in the main text.

The dynamics of the real part of the modes is very similar to the previous case (compare the top panels of Fig.8 and Fig.9). The difference is nevertheless evident in the imaginary part of the modes. First, as already mentioned, both the modes (real and imaginary part) remain hydrodynamic, in the sense that both the imaginary parts vanish at zero momentum. Second, the difference is evident also comparing the situation at large damping $\gamma \gg 1$ with that at large diffusion $D \gg 1$. In the first case, one of the two modes disappear from the low energy dynamics because it becomes overdamped, with $\mathrm{Im}(\omega) \sim -\gamma$ very large. In the second case, at large diffusion constant, the two modes also stop to interact but this second mode becomes now totally diffusive $\omega \sim -iDk^2$ and therefore still present in the low energy dynamics of the system. This second hydrodynamic mechanism is crucial in our discussion since the effects of diffusion are essential to provide a complete theoretical description of the experimental data.

Finally, in Fig.10, we show the Debye normalized absorption predicted by theory using the diffusive model. The position of the BP moves towards lower frequency by increasing the diffusion constant D. This dynamics is consistent with the correlation of the BP frequency with the Ioffe-Regel crossover that we discovered in Fig. 4. In the inset, we show also the dispersion relation of the phonon-polariton to emphasize that the BP frequency and the frequency of band flattening ω_{flat} defined in the main text do not coincide.

DATA AVAILABILITY

The data that supports the findings of this study are available within the article [and its supplementary material].

[1] M. Born and K. Huang, *Dynamical Theory of Crystal Lattices* (Oxford University Press, Oxford, 1954).
[2] R. Shuker and R. W. Gammon, Phys. Rev. Lett. **25**, 222 (1970).
[3] S. N. Taraskin, Y. L. Loh, G. Natarajan, and S. R. Elliott, Phys. Rev. Lett. **86**, 1255 (2001).
[4] A. I. Chumakov, G. Monaco, A. Monaco, W. A. Crichton, A. Bosak, R. Rüffer, A. Meyer, F. Kargl, L. Comez, D. Fioretto, H. Giefers, S. Roitsch, G. Wortmann, M. H. Manghnani, A. Hushur, Q. Williams, J. Balogh, K. Parliński, P. Jochym, and P. Piekarz, Phys. Rev. Lett. **106**, 225501 (2011).
[5] R. Milkus and A. Zaccone, Phys. Rev. B **93**, 094204 (2016).
[6] Y. Wang, L. Hong, Y. Wang, W. Schirmacher, and J. Zhang, Phys. Rev. B **98**, 174207 (2018).
[7] M. Baggioli and A. Zaccone, Phys. Rev. Research **2**, 013267 (2020).
[8] B. Rufflé, G. Guimbretière, E. Courtens, R. Vacher, and G. Monaco, Phys. Rev. Lett. **96**, 045502 (2006).
[9] H. Shintani and H. Tanaka, Nat. Mater. **7**, 870 (2008).
[10] Y. M. Beltukov, V. I. Kozub, and D. A. Parshin, Phys. Rev. B **87**, 134203 (2013).
[11] W. Schirmacher, G. Ruocco, and T. Scopigno, Phys. Rev. Lett. **98**, 025501 (2007).
[12] A. Marruzzo, W. Schirmacher, A. Fratalocchi, and G. Ruocco, Scientific Reports **3**, 1407 (2013).
[13] H. Mizuno, S. Mossa, and J.-L. Barrat, Proceedings of the National Academy of Sciences **111**, 11949 (2014), https://www.pnas.org/content/111/33/11949.full.pdf.
[14] S. Gelin, H. Tanaka, and A. Lemaître, Nature Materials **15**, 1177 (2016).
[15] B. Cui and A. Zaccone, Soft Matter **16**, 7797 (2020).
[16] A. Zaccone, Journal of Physics: Condensed Matter **32**, 203001 (2020).
[17] W. Schirmacher, V. Folli, C. Ganter, and G. Ruocco, Journal of Physics A: Mathematical and Theoretical **52**, 464002 (2019).
[18] M. Baggioli, R. Milkus, and A. Zaccone, Phys. Rev. E **100**, 062131 (2019).
[19] M. Baggioli and A. Zaccone, Physical Review Letters **122** (2019), 10.1103/physrevlett.122.145501.
[20] J. F. Gebbia, M. A. Ramos, D. Szewczyk, A. Jezowski, A. I. Krivchikov, Y. V. Horbatenko, T. Guidi, F. J. Bermejo, and J. L. Tamarit, Phys. Rev. Lett. **119**, 215506 (2017).
[21] M. Moratalla, J. F. Gebbia, M. A. Ramos, L. C. Pardo, S. Mukhopadhyay, S. Rudić, F. Fernandez-Alonso, F. J. Bermejo, and J. L. Tamarit, Phys. Rev. B **99**, 024301 (2019).

[22]A. Jeżowski, M. A. Strzhemechny, A. I. Krivchikov, N. A. Davydova, D. Szewczyk, S. G. Stepanian, L. M. Buravtseva, and O. O. Romantsova, Phys. Rev. B **97**, 201201 (2018).
[23]P. B. Allen, J. L. Feldman, J. Fabian, and F. Wooten, Philosophical Magazine B **79**, 1715 (1999).
[24]K. Huang, in *Selected Papers of Kun Huang* (World Scientific, 2000) pp. 50–56.
[25]K. Huang, Proceedings of the Royal Society of London Series A **208**, 352 (1951).
[26]R. Zwanzig, Journal of Statistical Physics **9**, 215 (1973).
[27]M. Born, *Atomic physics* (Blackie & Son, London, 1969).
[28]L. Landau and E. Lifshitz, *Electrodynamics of Continuous Media* (Pergamon Press, Oxford, 1960).
[29]P. B. Allen and J. L. Feldman, Phys. Rev. B **48**, 12581 (1993).
[30]R. C. Zeller and R. O. Pohl, Phys. Rev. B **4**, 2029 (1971).
[31]M. Baggioli and A. Zaccone, Phys. Rev. Lett. **122**, 145501 (2019).
[32]M. Baggioli and A. Zaccone, Phys. Rev. Research **1**, 012010 (2019).
[33]Y. M. Beltukov, V. I. Kozub, and D. A. Parshin, Phys. Rev. B **87**, 134203 (2013).
[34]L. Landau and E. Lifshitz, *Fluid Mechanics: Volume 6*, v. 6 (Elsevier Science, Amsterdam, 2013).
[35]G. Baldi, V. M. Giordano, G. Monaco, and B. Ruta, Phys. Rev. Lett. **104**, 195501 (2010).
[36]B. Ruzicka, T. Scopigno, S. Caponi, A. Fontana, O. Pilla, P. Giura, G. Monaco, E. Pontecorvo, G. Ruocco, and F. Sette, Phys. Rev. B **69**, 100201 (2004).
[37]L. Wang, L. Berthier, E. Flenner, P. Guan, and G. Szamel, Soft Matter **15**, 7018 (2019).
[38]N. Kryuchkov, L. Mistryukova, V. Brazhkin, and S. Yurchenko, Scientific Reports **9** (2019), 10.1038/s41598-019-46979-y.
[39]F. L. Galeener and P. N. Sen, Phys. Rev. B **17**, 1928 (1978).
[40]S. N. Taraskin, S. I. Simdyankin, S. R. Elliott, J. R. Neilson, and T. Lo, Phys. Rev. Lett. **97**, 055504 (2006).
[41]M. Kabeya, T. Mori, Y. Fujii, A. Koreeda, B. W. Lee, J.-H. Ko, and S. Kojima, Phys. Rev. B **94**, 224204 (2016).
[42]C. Kittel, *Introduction to Solid State Physics* (Wiley, New York, 2004).
[43]A. Ioffe and A. Regel, Progress in Semiconductors, edited by AF Gibson, (Heywood, London, 1960) **4**, 237 (1960).
[44]F. Wu and S. Das Sarma, Phys. Rev. Lett. **124**, 046403 (2020).
[45]T. Shibata, T. Mori, and S. Kojima, Spectrochimica Acta Part A: Molecular and Biomolecular Spectroscopy **150**, 207 (2015).
[46]W. Terao, T. Mori, Y. Fujii, A. Koreeda, M. Kabeya, and S. Kojima, Spectrochimica Acta Part A: Molecular and Biomolecular Spectroscopy **192**, 446 (2018).
[47]T. Mori, Y. Jiang, Y. Fujii, S. Kitani, H. Mizuno, A. Koreeda, L. Motoji, H. Tokoro, K. Shiraki, Y. Yamamoto, and S. Kojima, Phys. Rev. E **102**, 022502 (2020).
[48]S. Kojima and T. Mori, Ferroelectrics **500**, 183 (2016), https://doi.org/10.1080/00150193.2016.1214522.
[49]S. Kojima and T. Mori, AIP Conference Proceedings **1627**, 52 (2014), https://aip.scitation.org/doi/pdf/10.1063/1.4901657.
[50]T. Mori, H. Igawa, D. Okada, Y. Yamamoto, K. Iwamoto, N. Toyota, and S. Kojima, Journal of Molecular Structure **1090**, 93 (2015).
[51]R. Soto, *Kinetic Theory and Transport Phenomena*, Oxford master series in condensed matter physics (Oxford University Press, 2016).
[52]A. I. Akhiezer, J. Phys. (Moscow) **1**, 277 (1939).
[53]"Supplementary information available at...".
[54]M. Baggioli and A. Zaccone, Phys. Rev. Research **2**, 013267 (2020).
[55]B. Rufflé, G. Guimbretière, E. Courtens, R. Vacher, and G. Monaco, Phys. Rev. Lett. **96**, 045502 (2006).

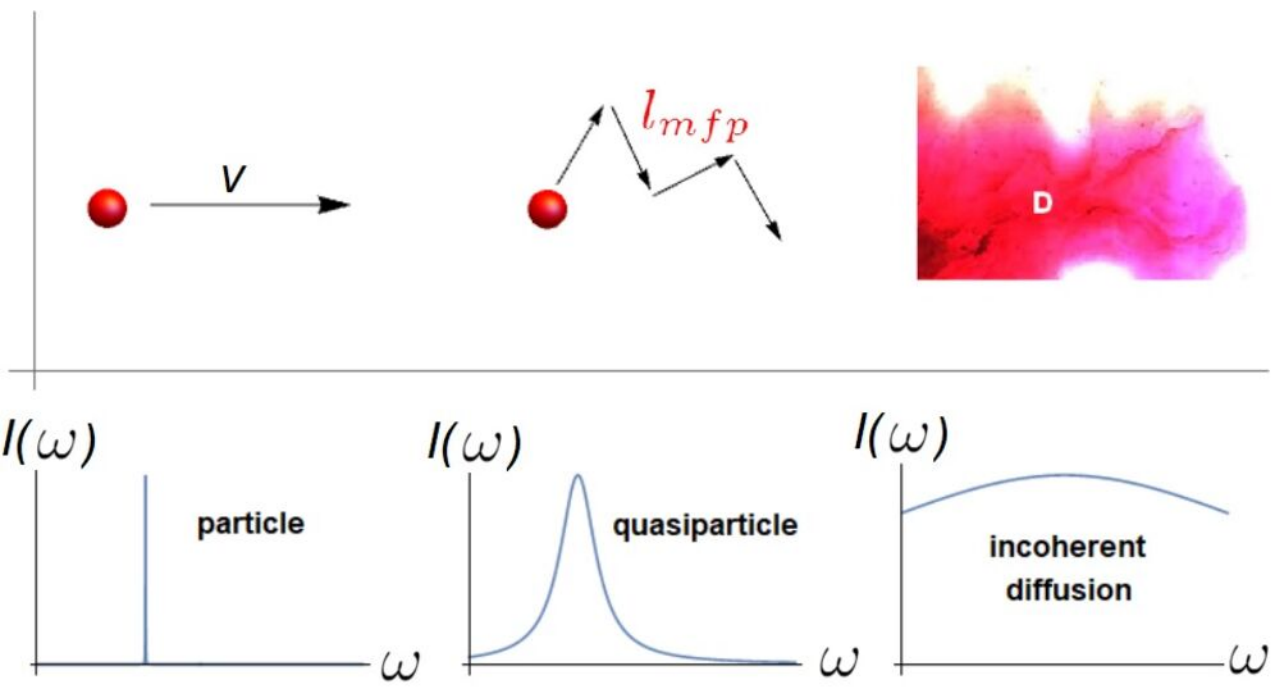
v
l_{mfp}
D
I(ω)
particle
ω
I(ω)
quasiparticle
ω
I(ω)
incoherent
diffusion
ω

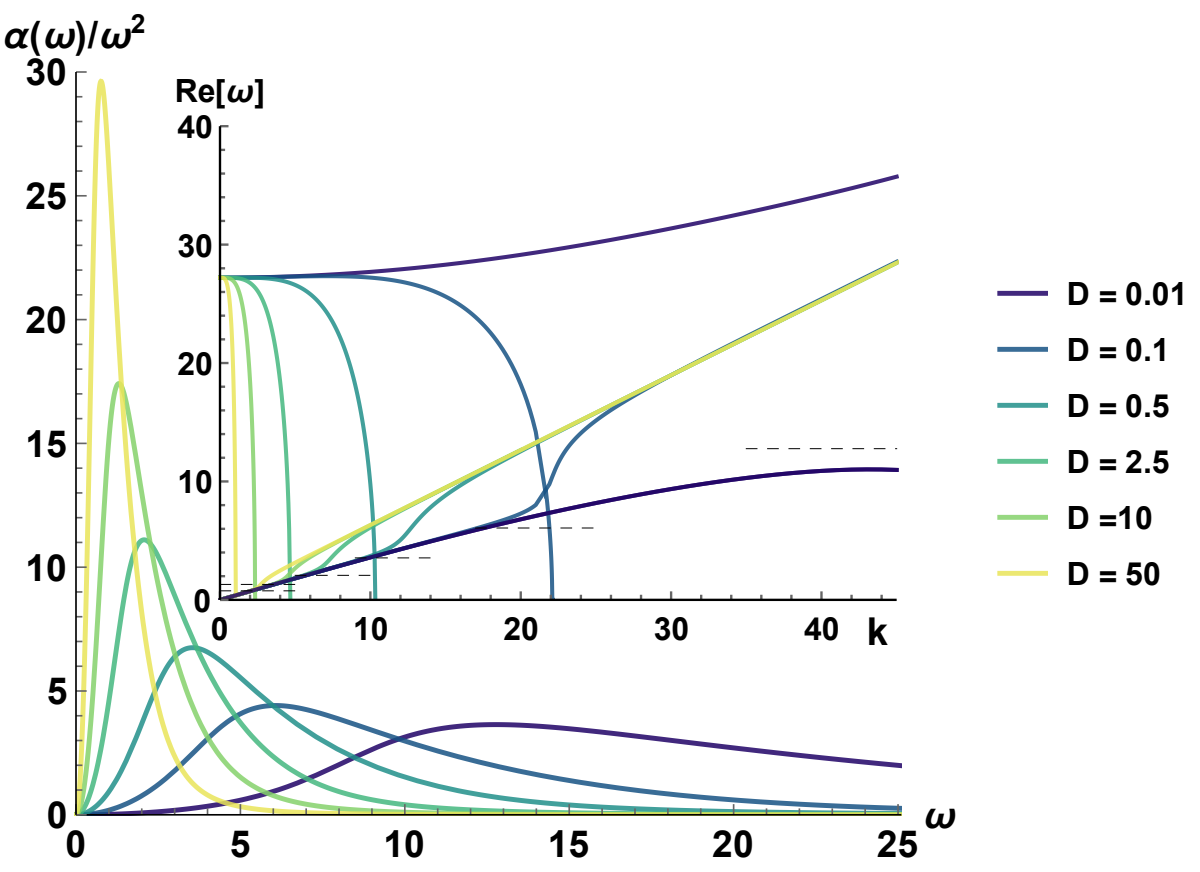
α(ω)/ω²
30
25
20
15
10
5
0
0
5
10
15
20
25
ω
Re[ω]
40
30
20
10
0
0
10
20
30
40
k
D = 0.01
D = 0.1
D = 0.5
D = 2.5
D =10
D = 50

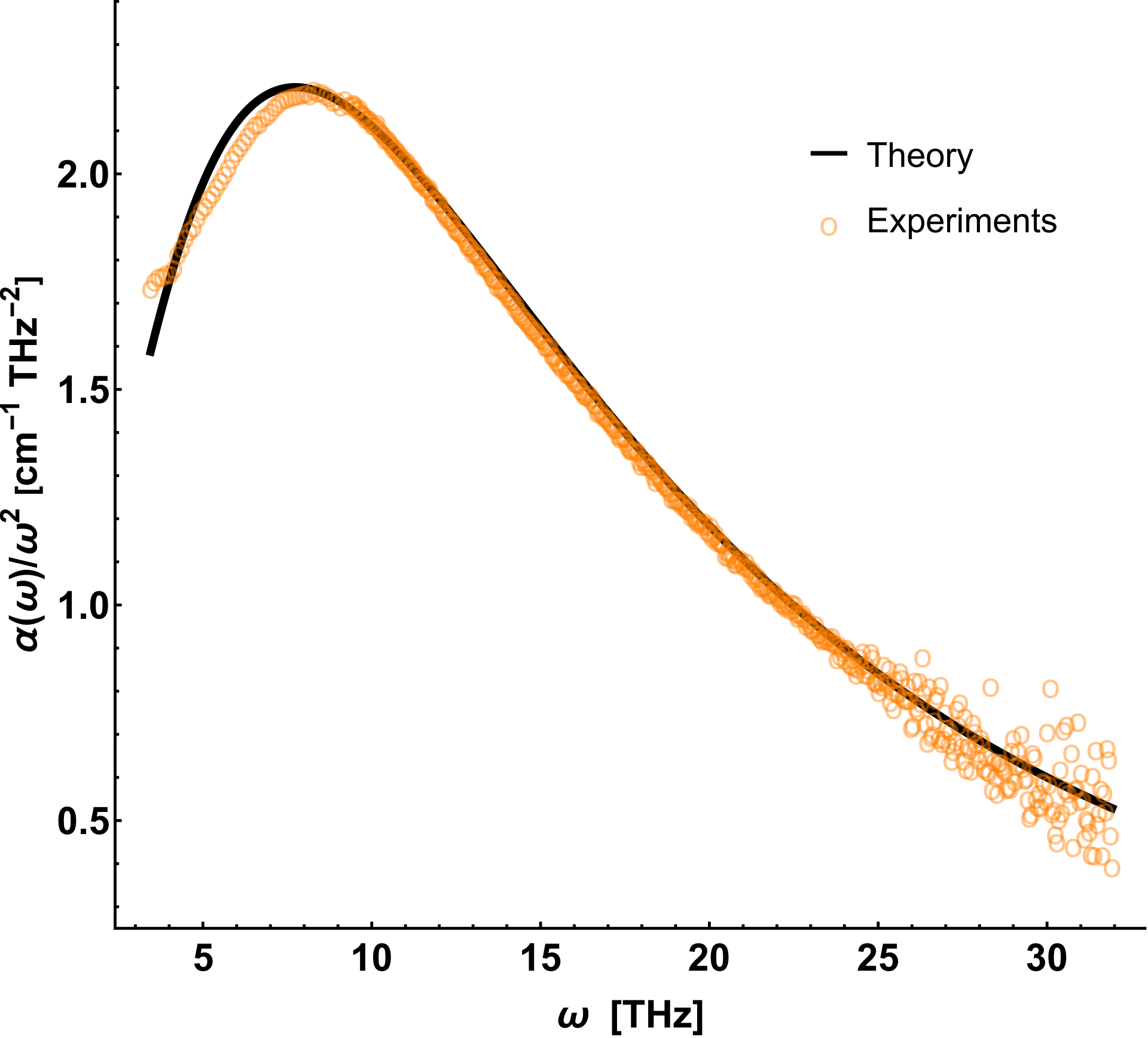
Theory
Experiments
2.0
1.5
1.0
0.5
5
10
15
20
25
30
α(ω)/ω² [cm⁻¹ THz⁻²]
ω [THz]

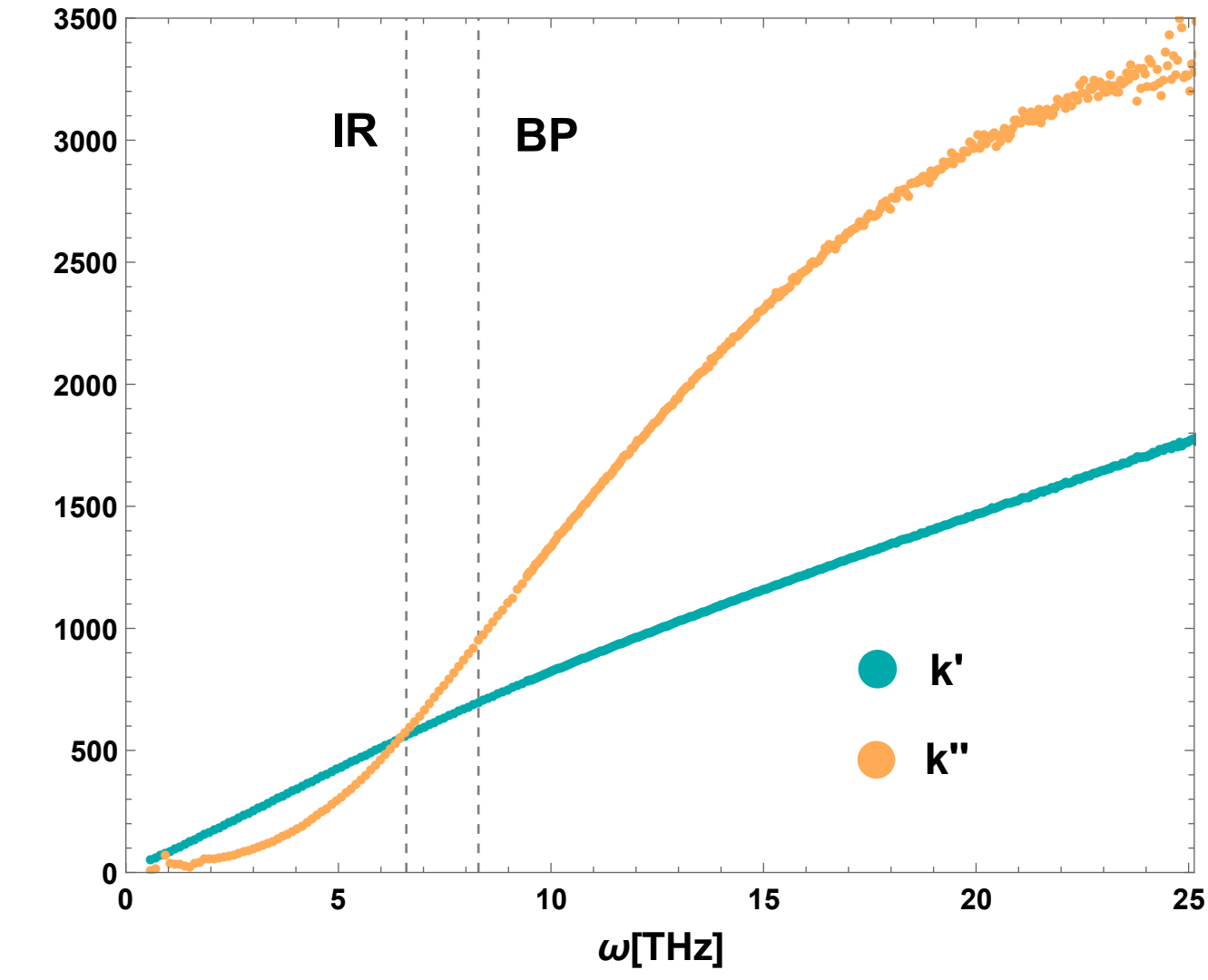
IR
BP
k'
k''
3500
3000
2500
2000
1500
1000
500
0
0
5
10
15
20
25
ω[THz]

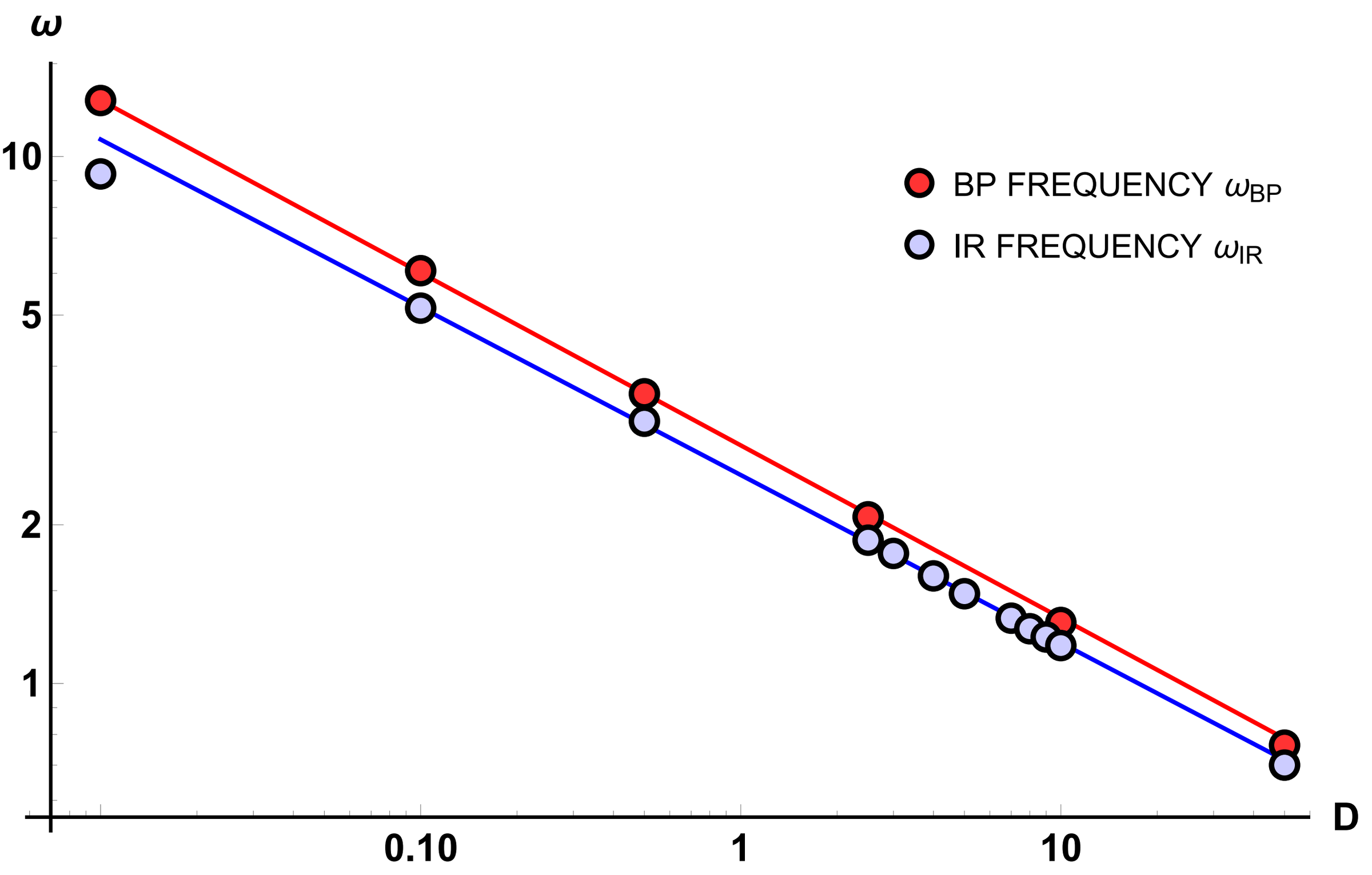
ω
10
5
2
1
0.10
1
10
D
BP FREQUENCY ω_{BP}
IR FREQUENCY ω_{IR}

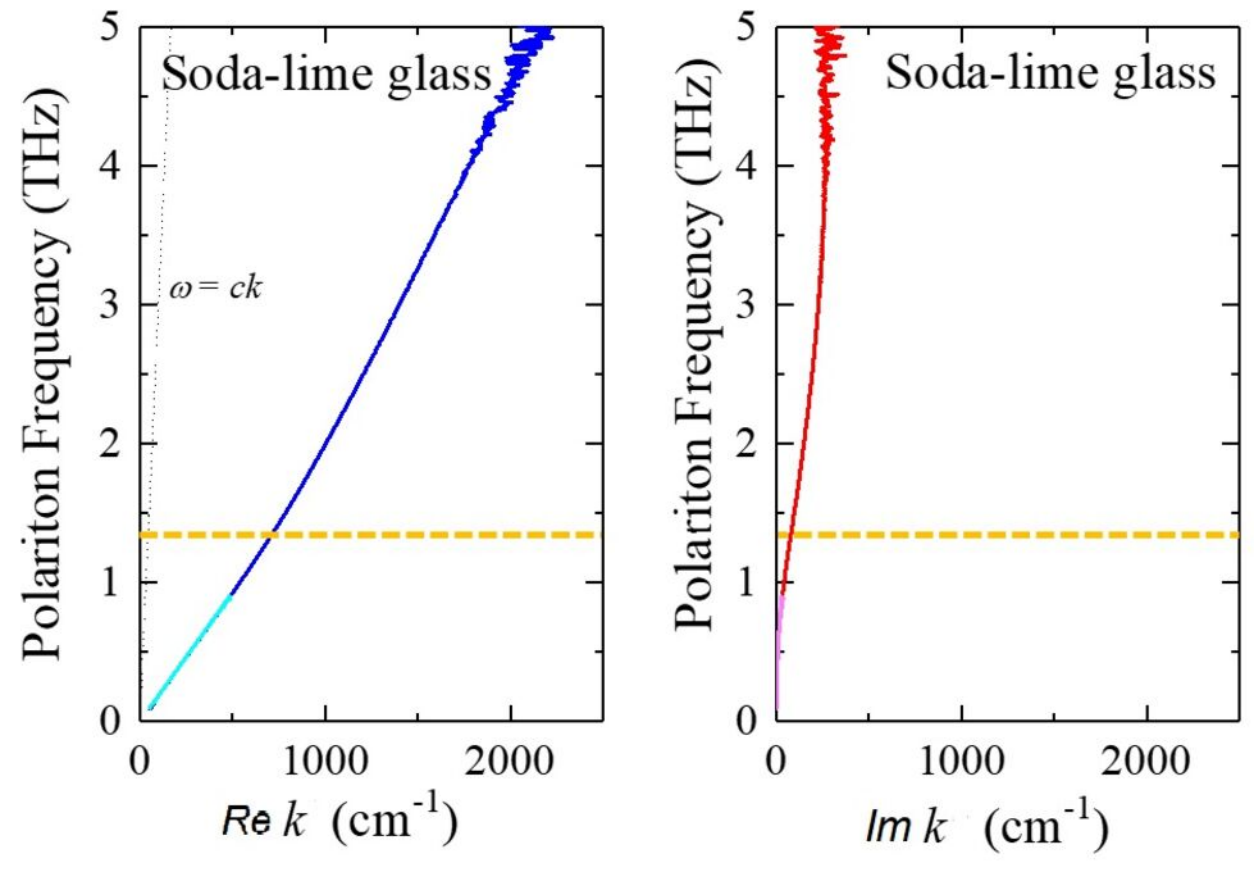
Soda-lime glass
Polariton Frequency (THz)
ω = ck
Re k (cm-1)
Soda-lime glass
Polariton Frequency (THz)
Im k (cm-1)

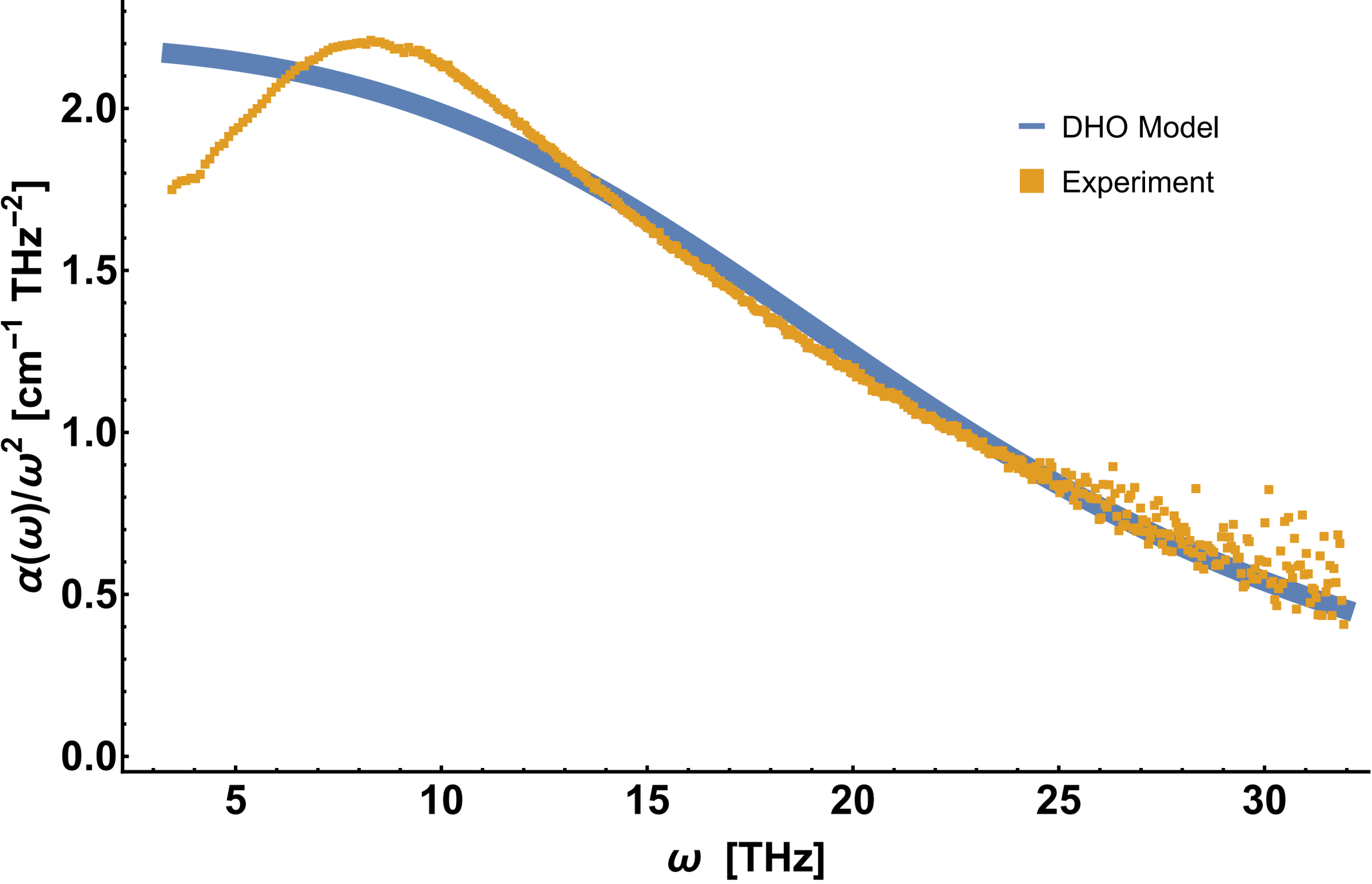
DHO Model
Experiment
$\alpha(\omega)/\omega^2$ [cm^{-1} THz^{-2}]
ω [THz]
0.0
0.5
1.0
1.5
2.0
5
10
15
20
25
30

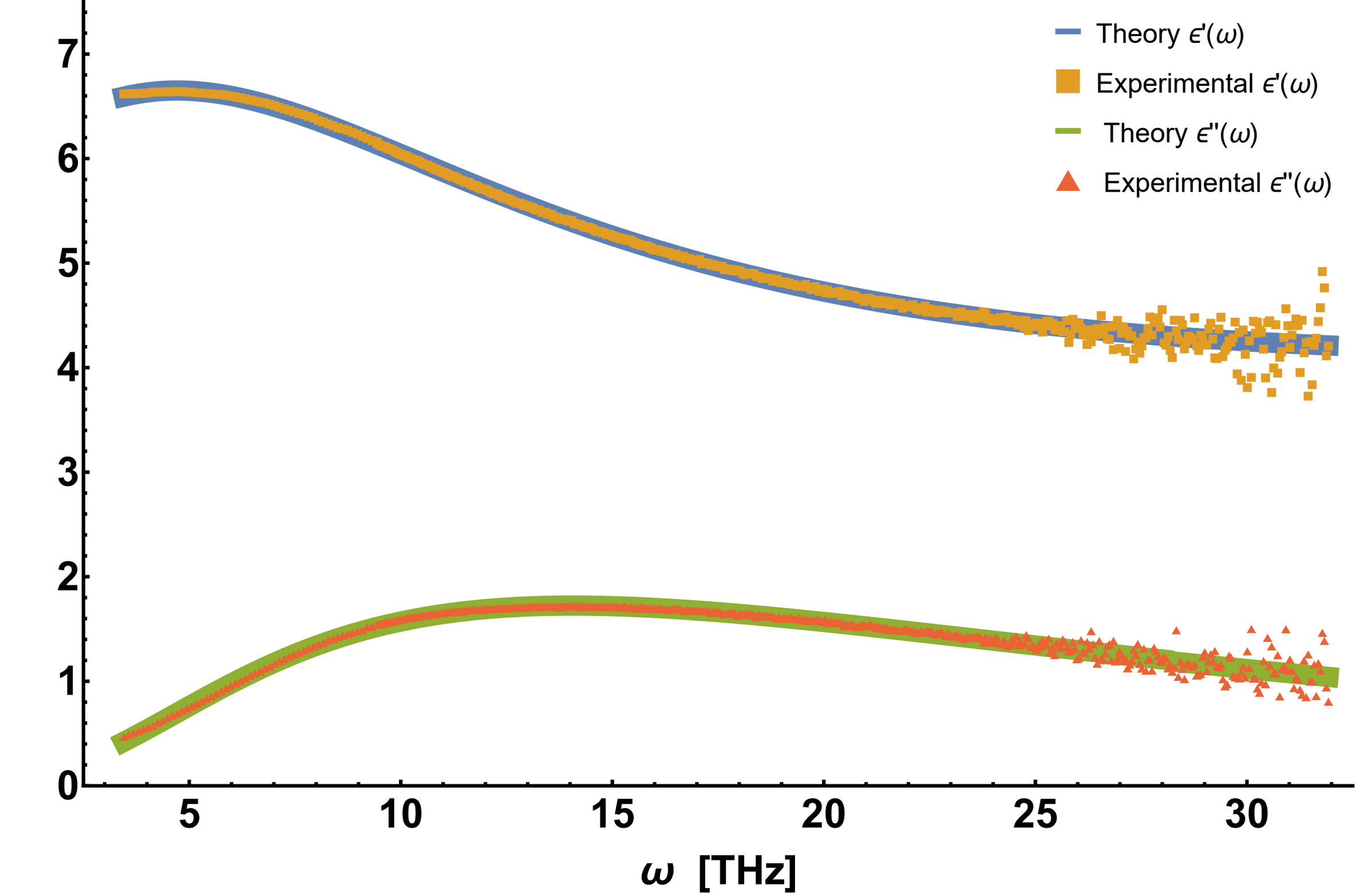
Theory $\epsilon'(\omega)$
Experimental $\epsilon'(\omega)$
Theory $\epsilon''(\omega)$
Experimental $\epsilon''(\omega)$
0
1
2
3
4
5
6
7
5
10
15
20
25
30
ω [THz]

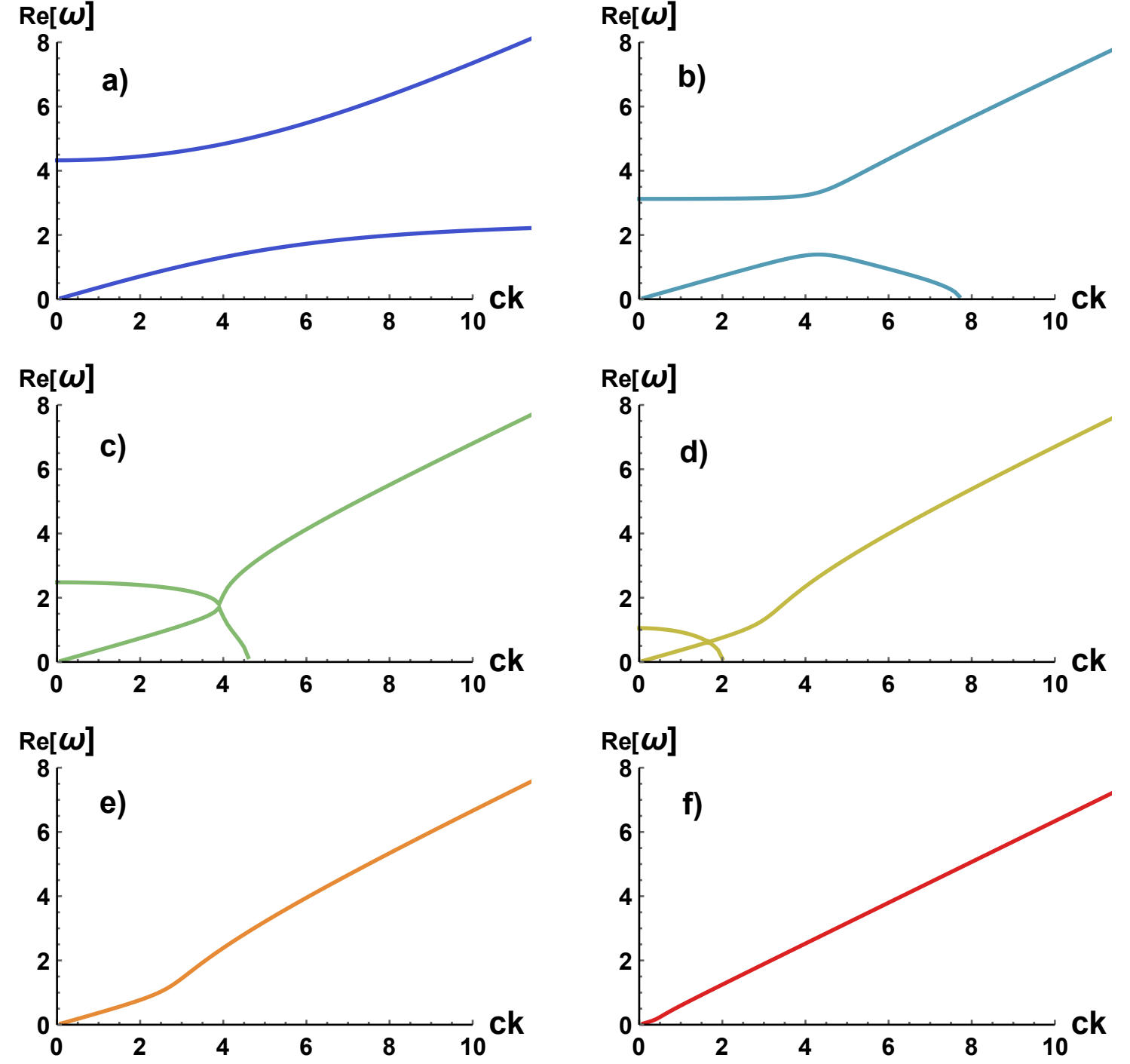
Re[ω]
a)
b)
c)
d)
e)
f)
ck
0
2
4
6
8
10

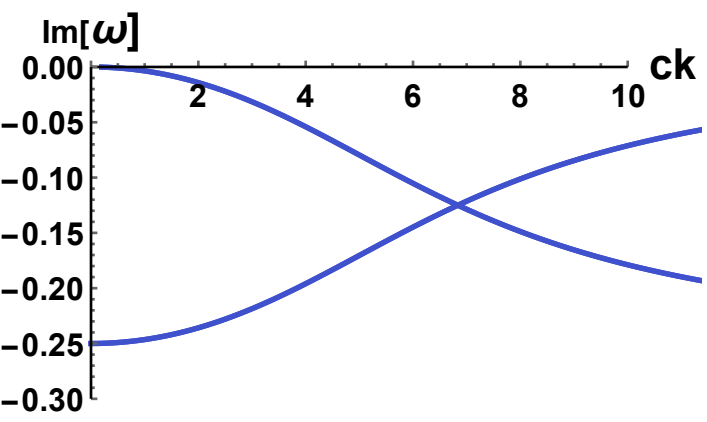
Im[ω]
ck
0.00
−0.05
−0.10
−0.15
−0.20
−0.25
−0.30
2
4
6
8
10

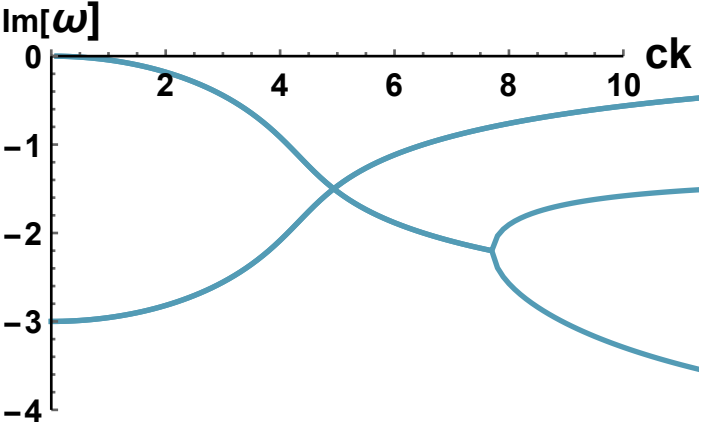
Im[ω]
ck
0
−1
−2
−3
−4
2
4
6
8
10

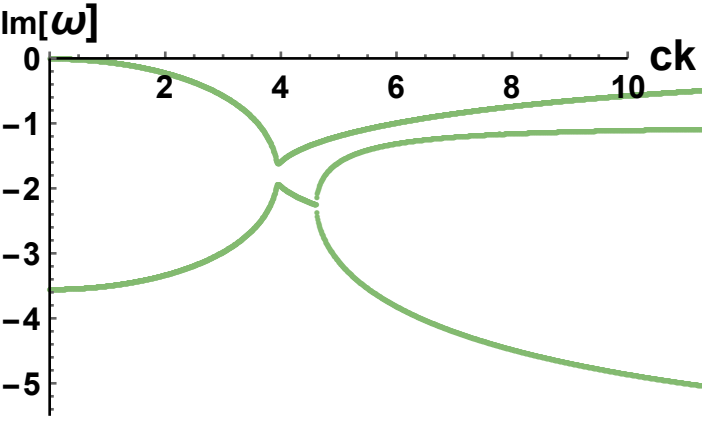
Im[ω]
ck
0
−1
−2
−3
−4
−5
2
4
6
8
10

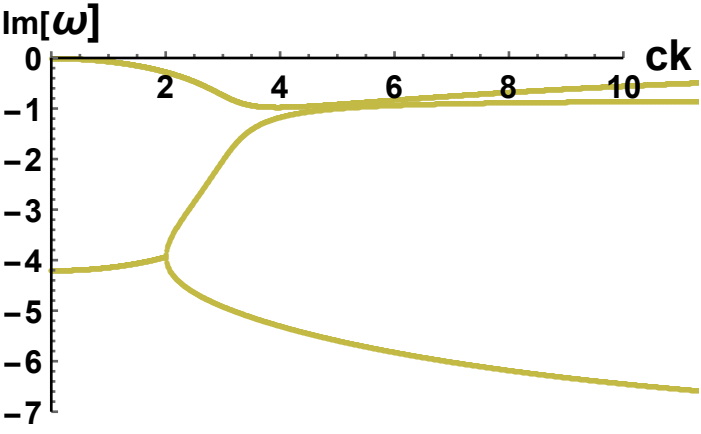
Im[ω]
ck
0
−1
−2
−3
−4
−5
−6
−7
2
4
6
8
10

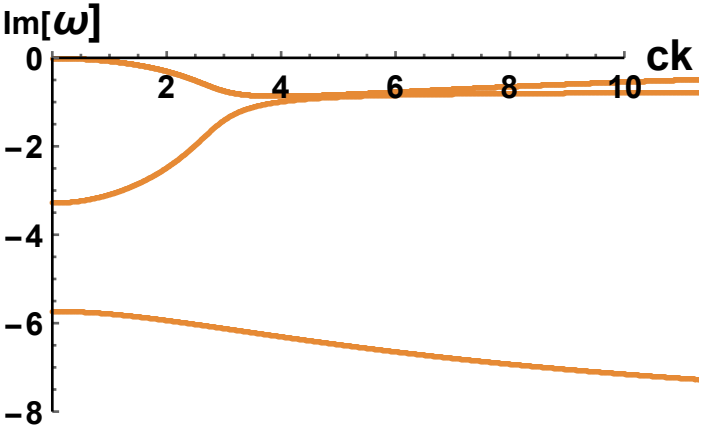
Im[ω]
ck
0
−2
−4
−6
−8
2
4
6
8
10

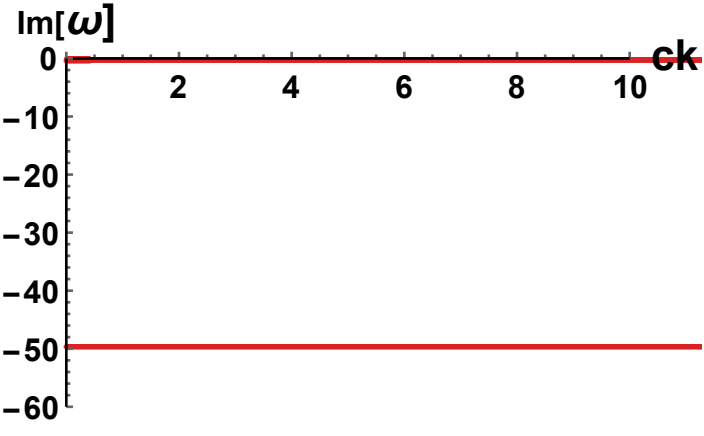
Im[ω]
ck
0
−10
−20
−30
−40
−50
−60
2
4
6
8
10

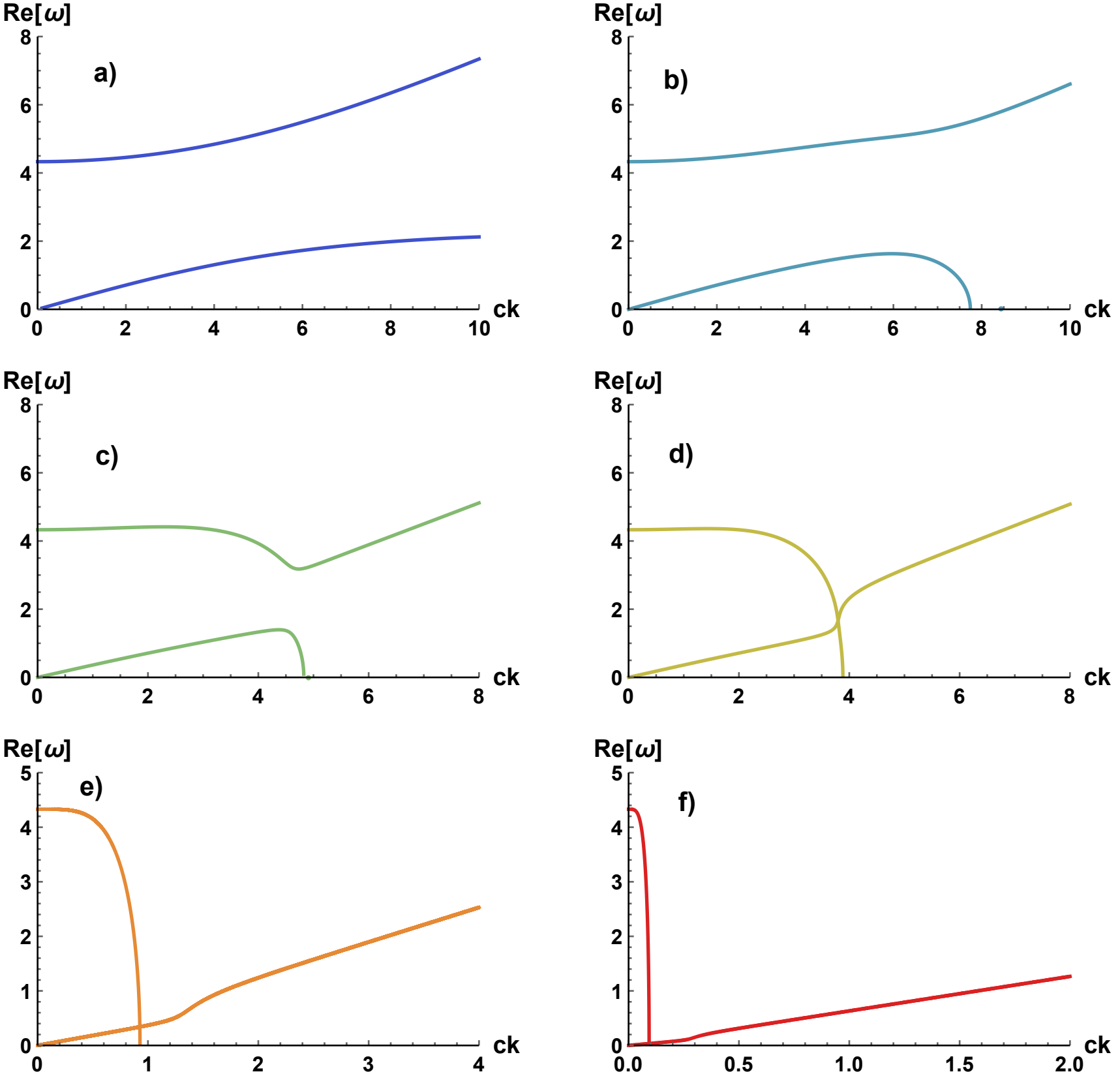
Re[ω]
a)
ck
Re[ω]
b)
ck
Re[ω]
c)
ck
Re[ω]
d)
ck
Re[ω]
e)
ck
Re[ω]
f)
ck

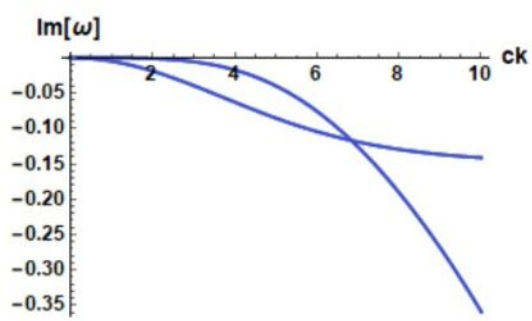
Im[ω]
ck
2
4
6
8
10
−0.05
−0.10
−0.15
−0.20
−0.25
−0.30
−0.35

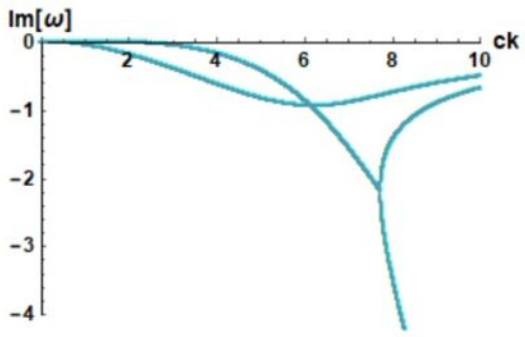
Im[ω]
ck
0
2
4
6
8
10
−1
−2
−3
−4

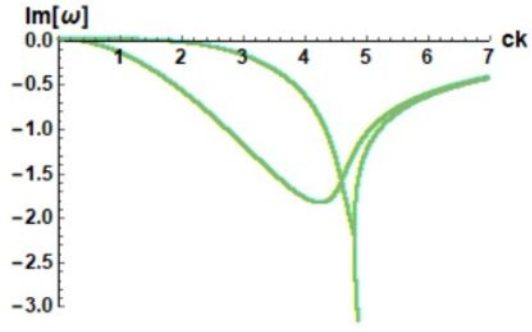
Im[ω]
ck
0.0
1
2
3
4
5
6
7
−0.5
−1.0
−1.5
−2.0
−2.5
−3.0

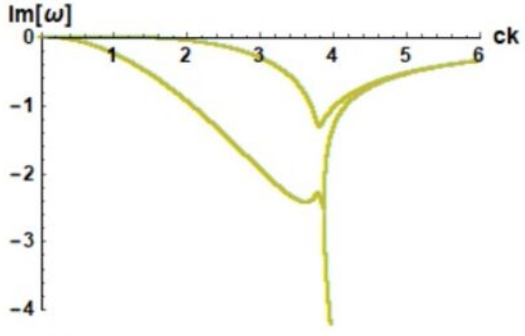
Im[ω]
ck
0
1
2
3
4
5
6
−1
−2
−3
−4

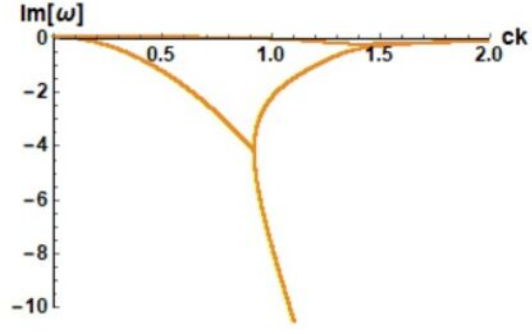
Im[ω]
ck
0
0.5
1.0
1.5
2.0
−2
−4
−6
−8
−10

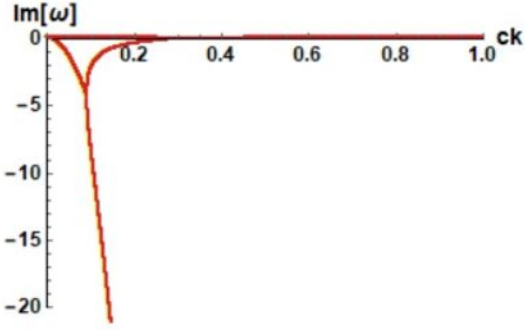
Im[ω]
ck
0
0.2
0.4
0.6
0.8
1.0
−5
−10
−15
−20